Journal of Saudi Chemical Society (2014) **18**, 69–76

King Saud University

Journal of Saudi Chemical Society

www.ksu.edu.sa
www.sciencedirect.com

ORIGINAL ARTICLE

Structural, textural and catalytic properties of pure and Li-doped NiO/Al_2O_3 and CuO/Al_2O_3 catalysts

Sheikha S. Ashour *

Chemistry Department, Applied Science College, Umm El-Qura University, Makkah, PO Box 1847, Saudi Arabia

Received 15 March 2011; accepted 29 May 2011
Available online 6 June 2011

KEYWORDS

Catalytic Properties;
Li-doped NiO/Al_2O_3;
CuO/Al_2O_3

Abstract Pure and Li-doped NiO/Al_2O_3 and CuO/Al_2O_3 catalysts were prepared to contain 2, 4 and 8 wt.% of Ni and Cu, respectively. The structural properties were determined using DTA, XRD and FTIR techniques, and the textural properties of the catalysts were determined from their adsorption–desorption isotherms of nitrogen at 77 K. The chemisorption of hydrogen at 473–823 K with the pre-reduced catalysts was measured. The data obtained allowed the determination of the metal surface area, S (m^2/g); the percentage of metal distribution, R; and the diameter of metal crystallite, d (nm). The amount of surface acidity, measured in mmol/g, was determined from the amount of chemisorbed pyridine necessary to completely inhibit the catalytic dehydration (DHD) of isopropanol. The conversion of isopropanol at 533–623 K was investigated using the micro-catalytic pulse technique. DTA, XRD and FTIR indicated that NiO and CuO exist as separate phases with crystallite sizes too small to be detected. No evidence has been gathered to indicate the existence of an aluminate phase.

With the increase of metal loading, the surface area decreased whereas the total pore volume and the mean pore radius increased. Conversion of iso-propanol to propene proceeded via (DHD) on surface acid sites, and conversion of isopropanol to acetone proceeded via dehydrogenation (DHG) on redox sites. DHD and DHG exhibited first-order kinetics, and the rates of both reactions increased with temperature, with the latter being more temperature-dependent.

1. Introduction

Mixed oxide catalysts often have catalytic properties that are superior to those of pure oxides (El-Sharkawy et al., 2000; Ashour, 2007). The surface and catalytic properties of different transition metals and transition metal oxides are improved by their loading onto alumina (Leyrer et al., 1986; Airaksinen et al., 2003).The extent of the improvement depends upon the method of preparation, chemical composition, and the thermal treatment temperature (Mikhail et al., 1979; Youssef and Youssef, 1991). In many instances, the metal particles are distributed on the support that offers a means of retaining

* Tel.: +966 504532086; fax: +966 2 5614003.
E-mail address: sheikha_s_ashour@hotmail.com

Peer review under responsibility of King Saud University.
doi:10.1016/j.jscs.2011.05.016

Production and hosting by Elsevier

the metal particles in a state that is both stable toward agglomeration and accessible to reactants (Harlin et al., 2001). The support also enables the preparation of a catalyst that has mechanical properties that facilitate convenient handling (Vishwanthan et al., 1991).

Alumina possesses a high surface area; and therefore, transition metal oxides supported on alumina always exist in a high dispersion form. Upon calcinations at or above 823 K, chemical interactions between alumina and the transition metal oxides may take place. Depending upon the nature of the transition metal oxide, the composition and the conditions of preparation, two types of reactions are expected to occur concurrently: the formation (at least at the surface) of metal aluminate and the formation of a stable well-dispersed metal oxide. Doping with a small amount of certain cations, including Li^+, Na^+, Ca^{2+}, Ga^{3+} and Ge^{4+}, influenced the chemical interaction between loaded oxides and their supports (Lycourghiotis et al., 1982).

The conversion of alcohols has been employed as a catalytic test for the study of dual function catalysts. The catalytic dehydration (DHD) and dehydrogenation (DHG) of isopropanol is important for the production of acetone and propene, respectively (Youssef and Mostafa, 1988; Youssef et al., 1998).

The present investigation reports the effects on the textural properties and surface acidity of NiO/Al_2O_3 and CuO/Al_2O_3 catalysts caused by the doping of alumina with a small amount of Li^+. The factors controlling the textural properties, catalytic activity and catalytic selectivity in the conversion of isopropanol are discussed.

2. Experimental

2.1. Catalysts

Alumina was prepared by precipitation from an $Al(NO_3)_3{\cdot}9H_2O$ solution using 2 M NH_4OH at 243 K and pH 8. The precipitate was washed several times with doubly distilled water until free from NO_3^- ions and then dried at 413 K until a constant weight was obtained. Samples of dried alumina were impregnated in hydrated nickel nitrate of different concentrations and were then dried and calcined at 823 K. The calcined catalysts N2, N4 and N8 were found to contain 2, 4 and 8 wt.% Ni, respectively, using atomic absorption spectroscopy (AA) in a Perkin–Elmer 1700 apparatus. Similarly, C2, C4 and C8 catalysts were prepared to contain 2, 4 and 8 wt.% Cu, respectively. Two samples of alumina were doped with $LiNO_3$ in which the amount of lithium expressed as wt.% Li_2O was equal to 3.7. Two samples of Li-doped alumina were used to prepare catalysts containing 8 wt.% Ni or Cu, i.e., LN8 and LC8, respectively.

2.2. Techniques

Differential thermal analysis (DTA) of non-calcined selected samples was carried out using a Netzsch-Geratebau thermal analyzer (STA 409, type 6223). The rate of heating was 10 deg/min. X-ray diffraction (XRD) of some calcined samples was performed using a Philips diffractometer (type PW 1390). The patterns were obtained using Ni-filtered copper radiation $\lambda = 1.5405$ Å) at 36 kV and 10 mA with a scanning speed of 1° in 20 min^{-1}. The FTIR spectroscopic investigations of a few calcined samples were carried out using an ATI Mattson 5000 FTIR spectrometer and the KBr disc technique. Chemisorption of hydrogen was carried out using a conventional high vacuum apparatus with catalysts reduced in situ at 673 K for 6 h in a hydrogen flow, followed by outgassing for 6 h at the same temperature. The catalyst was cooled to 473 K and left for 3 h before hydrogen adsorption was carried out at the same temperature. The linear portion of the isotherm was extrapolated to zero pressure to discount the physisorption.

A micro-catalytic pulse technique was used to determine the surface acidity and catalytic activity of each catalyst. For the measurement of surface acidity, each catalyst was activated at 723 K for 3 h in a nitrogen stream, and then a series of pyridine doses was injected onto the catalyst at 593 K. The effect of the pyridine on the conversion of isopropanol to propene was examined after each injection.

3. Result and discussion

3.1. Structural properties

DTA curves of pure non-calcined alumina and non-calcined N4, N8, C4 and C8 are shown in Fig. 1. For all of the samples, two endotherms are observed at 366–429 K and at 559–680 K. The low temperature endotherms are attributed to the loss of physisorbed water. The area of these endotherms decreased with the increase of metal loading. The endotherms at 559–680 K are mainly ascribed to the loss of lattice water and partially to the decomposition of the remaining nitrates (Youssef et al., 1998). No exotherms arising from solid–solid interactions or the formation of an aluminate phase were observed, and such exotherms may require thermal treatment at

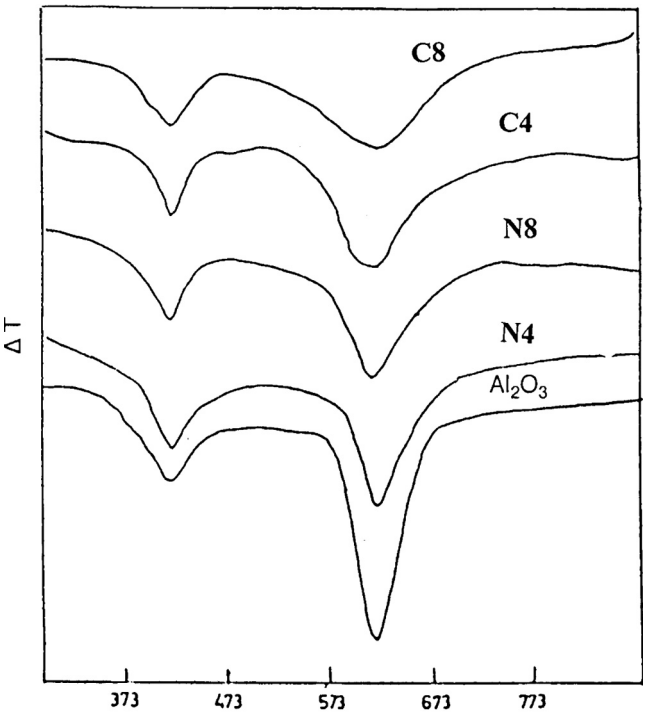

Figure 1 DTA curves of non-calcined alumina, N4, N8, C4 and C8.

temperatures higher than 680 K. For pure alumina, the 559–680 K endotherm is symmetrical with the minimum located at 598 K. For the supported metal catalysts, the 559–680 K endotherms are relatively broad and less symmetrical.

The XRD patterns of pure alumina and metal-supported catalysts calcined at 823 K (not illustrated) are all identical, indicating the absence of metal oxide phases or aluminate phases. This may be attributed to the absence of NiO or CuO particles of sufficient size to allow for their detection by this technique. This effect has been previously reported for CuO/Al_2O_3 systems with CuO content less than 16 wt.% (Sivaraj and Kanatarao, 1988). The high surface area of alumina allows for the high dispersion of the supported metal oxide crystallites (El-Nabarawy, 1997).

The FTIR spectra of pure alumina, Li-doped alumina, N8 and C8 samples (not illustrated) showed the following bands: broad bands centered at 3450 cm^{-1}, which were assigned to OH-combined water; bands at 3420 cm^{-1}, which were assigned to OH stretching; and less developed bands in the range of 606–890 cm^{-1}, which were ascribed to different vibration modes of H_2O, i.e., wagging, twisting and scissoring (Nakamoto, 1970). The bands ascribed to metal–oxygen bond vibrations were located in the range of 652–973 cm^{-1}. Specifically, the bands at 973, 756, 652 and 658 cm^{-1} were assigned to Li–O, Al–O, Ni–O and Cu–O, respectively, and verified with quantum mechanical calculations that incorporated Zibert's rule and Hook's rule.

3.2. Textural properties

Using catalysts that were calcined at 823 K, the adsorption of nitrogen at 77 K was found to be rapid, and the equilibrium was reached in 30 min. This result indicates the absence of ultra-fine pores in which adsorption may be controlled by activated diffusion. The isotherms lie between type II and type IV according to the classification of Sing et al. (1985). The desorption and adsorption branches meet at some intermediate relative pressure, giving a closed hysteresis loop. Representative adsorption-desorption isotherms are shown in Fig. 2. The BET equation (Brunauer et al., 1938) was applied, and the specific surface areas S_{BET} (m^2/g) were calculated. The total pore volume V_T (ml/g) and the mean pore radius r_m were also calculated for each catalyst (Table 1). Also included in this table are the surface areas determined by the α-method of Sing (1967), which allows for the determination of surface areas located in micropores and non-micropores, S_m^{α} and S_n^{α} (m^2/g), respectively, as well as the micropore and the non-micropore volumes, V_m^{α} and V_n^{α} (ml/g), respectively.

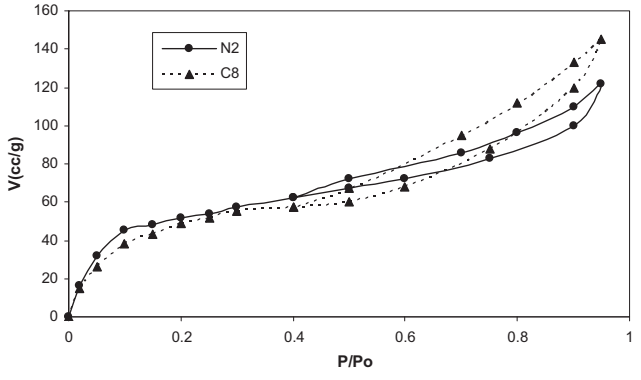

Fig. 2 Representative adsorption desorption isotherms of nitrogen at 77 K.

Table 1 reveals the following: (i) the values of S_{BET} are comparable to those of S_{α}, which may refer to the precise determination of the present surface area; (ii) the surface area decreased, whereas the total pore volume and the mean pore radius increased with the increase of metal oxide loading, which may indicate that metal loading is associated with pore widening; and (iii) generally, the volume of micropores decreased, whereas that of non-micropores increased with the increase of metal loading, although this was not true for catalysts supported on Li-doped alumina.

3.3. Chemisorption of hydrogen

The hydrogen uptake of each catalyst is shown in Table 2. These values facilitated the determination of some interesting adsorption parameters related to the catalytic performance. These parameters include the metal surface area, S; the dispersion, R; and the crystallite size, d, of the metal (Ni or Cu). Two expressions may be used for the metal surface area: (i) S (m^2/g(metal)) = $H_{ads.}/N \times$ metal content (%) and (ii) S (m^2/g(catalyst)) = $H_{ads.}/N$. In both expressions, N equals the number of surface Ni or Cu atoms/m^2 and equals 1.54×10^{19} for Ni and 1.49×10^{19} for Cu (Anderson, 1957).

The expressions for dispersion, R, and crystallite size, d, are as follows: (i) R = no of metal atoms on the support (%)/total no of metal atoms in the catalyst, and (ii) $d = 6 \times 10^3/\rho S$ where ρ is the density (g/cm^3) and equals 8.9 for Ni and 8.93 for Cu.

The parameters S, R, and d are listed in columns 4–7 of Table 2, respectively. Column 8 of Table 2 gives % DHG of isopropanol at 623 K and a flow rate of 25 cm^3/min.

Table 1 Textural properties of the catalysts as determined from nitrogen adsorption at 77 K.

Catalyst	S_{BET} (m^2/g)	V_T (ml/g)	r_m (nm)	S_{α} (m^2/g)	S_m^{α} (m^2/g)	S_n^{α} (m^2/g)	V_m^{α} (ml/g)	V_n^{α} (ml/g)
N2	232	0.190	1.64	216	114	102	0.120	0.070
N4	221	0.200	1.81	210	111	99	0.133	0.067
N8	198	0.236	2.38	189	92	97	0.177	0.059
LN8	221	0.213	2.27	182	83	99	0.152	0.061
C2	240	0.193	1.61	227	109	118	0.119	0.074
C4	228	0.201	1.76	219	101	118	0.130	0.071
C8	202	0.225	2.23	196	97	99	0.160	0.063
LC8	194	0.209	2.15	187	85	102	0.146	0.063

Table 2 Chenisorption of hydrogen at 473 K and % DHG of isopropanol at 623 and flow rate = 25 cm^3/min.

Catalyst	$N_t \times 10^{19}$/g(cat)	H_2 ads. (μmol/g)	S (m^2/g(met.))	S (m^2/g(cat.))	R (%)	d (nm)	% DHG
N2	20.50	0.141	551.2	11.02	82.8	1.22	21
N4	41.00	0.242	473.0	18.92	71.1	1.43	37
N8	82.00	0.355	346.9	27.75	52.2	1.94	54
LN8	82.00	0.350	342.0	27.36	51.4	1.97	52
C2	18.95	0.154	602.0	12.04	97.8	1.08	25
C4	37.90	0.282	551.0	22.04	89.6	1.18	41
C8	75.80	0.375	366.0	29.30	39.7	1.78.	6.1
LC8	75.80	0.368	360.0	28.80	58.4	1.81	6.2

Inspection of Table 2 reveals the following: (i) S (m^2/g(metal)) and R decreased, whereas S (m^2/g(catalyst)) and d increased with the increase of metal loading; (ii) the effect of doping with Li_2O on the chemisorption of hydrogen was very limited, and no pronounced effects on the sorption parameters or on % DHG were observed; and (iii) % DHG increased with the increase of hydrogen uptake and with the increase of S (m^2/g(catalyst)). A satisfactory straight line passing through the origin was obtained by plotting % DHG versus S (m^2/g(catalyst)) (Fig. 3).

3.4. Surface acidity

The conversion of isopropanol proceeds via DHD and DHG. The catalytic DHD proceeds on surface acid sites to give propene, whereas the catalytic DHG of this alcohol takes place on redox sites to furnish acetone (Bassett and Habgood, 1960). Surface acidities were determined using the poisoning method and application of the equation of Panchenkov and Lebedov (Bassett and Habgood, 1960). Determination of the amount of pyridine that completely inhibits the DHD activity of the catalyst α was effected through the equation $A_p/A_o = 1 - \alpha C_p$ where A_p is the DHD activity of the poisoned catalyst, A_o is the DHD activity of the fresh catalyst, α is the poisoning coefficient, and C_p is the poison concentration. Plots of A_p/A_o versus C_p, i.e., the poisoning isotherm (not illustrated), enabled the determination of the surface acidities of NiO/Al_2O_3 and Cu/Al_2O_3 catalysts, which were pre-calcined at 823 K (Table 3). Also included in Table 3 are the % DHD at 623 K and a flow rate of nitrogen carrier gas measured at F^o = 25 cm^3/min. Table 3 reveals that the following: (i) the surface acidity decreased, whereas the poisoning coefficient α increased with the increase of metal oxide loading; (ii) for the same loading, higher surface acidities were measured with CuO/Al_2O_3 catalysts compared with their NiO/Al_2O_3 counterparts; (iii) the surface acidities of Li-doped catalyst are considerably lower than those of non-doped ones; and (iv) % DHD is directly proportional to the amount of surface acidity, as shown by a straight line passing through the origin, which represents the relationship between A (μmol/g) and % DHD (Fig. 4). These results suggest that the DHD of alcohols takes place on the surface acid sites on the catalyst.

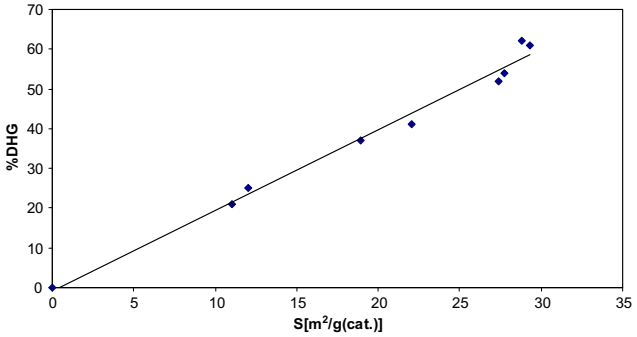

Fig. 3 % dehydrogenation (DHG) of isopropanol at 623 K and flow rate = 25 cm^3/min versus S (m^2/g(cat.)).

3.5. Catalytic conversion of isopropanol

The catalytic conversion of isopropanol at 533–623 K under a flow rate of 25–50 cm^3/min was investigated over the N4, N8, C4 and C8 catalysts. This allowed for the determination of the kinetics of DHD and DHG and the calculation of the activation energy, E_a (kJ mol^{-1}).

Table 3 Surface acidity as determined from pyridine chemisorption and % DHD of isopropanol at 623 K. Flow rate of the nitrogen gas carrier = 25 cm^3/min.

Catalyst	a (mmol/g)	N_{acid} sites/g $\times 10^{20}$	N_{acid} sites/$cm^2 \times 10^{14}$	(α)	% DHD
N2	0.75	4.52	1.95	0.36	41
N4	0.60	3.61	1.63	0.44	33
N8	0.26	1.56	0.79	1.03	15
LN8	0.10	0.60	0.32	2.67	7
C2	0.90	5.42	2.26	0.25	53
C4	0.71	4.27	1.87	0.30	47
C8	0.28	1.69	0.84	1.37	17
LC8	0.12	0.72	0.37	4.00	8

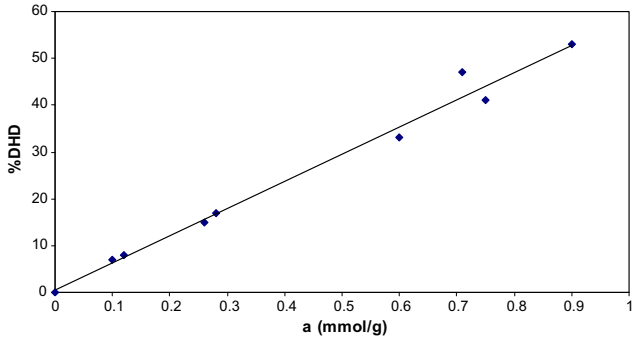

Fig. 4 % dehydration (DHD) of isopropanol at 623 K and flow rate = 25 cm^3/min versus a (mmol/g).

3.6. Catalyst selectivity

The selectivity of a catalyst towards a particular reaction is estimated by dividing the respective conversion to a certain product x (C_x) by the total conversion C. Thus, the selectivities towards propene and acetone were calculated from the following equations: (i) $C = C_p + C_a$, (ii) $S_p = C_p/C$, and (iii) $S_a = C_a/C$. In these equations, C_p = % propene generated; C_a = % acetone generated; and S_p and S_a are propene and acetone selectivities, respectively. Table 4 lists all the above-mentioned catalytic parameters. Table 4 reveals the following: (i) the total conversion of isopropanol to propene and acetone increased continuously with the increase of the reaction temperature; and (ii) generally, the total conversion decreased with the increase of the flow rate of the nitrogen carrier gas and also with the increase of metal oxide loading. The increase of metal oxide loading is associated with a pronounced decrease in surface acidity and a less pronounced increase in dehydrogenation activity. The result is, therefore, a decrease in the total conversion with the increase of metal oxide loading.

3.7. Reaction kinetics

The catalytic conversion of isopropanol over NiO/Al_2O_3 and CuO/Al_2O catalysts was found to fulfill the conditions necessary for first-order reactions (El-Jamal et al., 1988), in which the reactant partial pressure is low, i.e., the fractional conversion of the reactant to products is independent of the pressure and the rate of the adsorption is faster than the rate of the reaction, the latter being the rate-determining step. Quantitative treatment of the data was carried out by the application of the Bassett–Habgood equation for first-order reactions. Representative plots of Ln $1/1 - x$ versus $1/F^o$ are shown in Fig. 5a for the DHD of isopropanol at 533 K and a flow rate of 2–50 cm^3/min over N4 and C4. Satisfactory straight lines passing through the origin were obtained, verifying the reactions adhered to first-order kinetics. The same was found to be true for the DHG of the same alcohol. Representative plots of Ln $1/1 - x$ versus $1/F^o$ for DHG onto N8 and C8 are shown in Fig. 5b.

For first-order kinetics, the slope of the linear plot passing through the origin is equivalent to the rate constant k (min^{-1}). Table 5 lists the apparent rate constants for DHD (k_{DHD}) and DHG (k_{DHG}) at 533–623 K.

The Arrhenius equation was used to estimate the apparent activation energies for DHD and DHG of isopropanol onto N4, N8, C4 and C8. The values of the activation energies, which are obtained from Figs. 6a and 6b, are listed in Table 6. The values of the activation energies are small, indicating that a small increase in the conversion temperature of isopropanol may be associated with a pronounced increase in the conversion of this alcohol to propene and acetone. The activation energies for DHG are slightly higher than those for DHD.

3.8. Reaction mechanism

It has been already mentioned that the catalytic conversion of isopropanol over the present catalysts takes place via DHD to propene and DHG to acetone. This agrees with previously reported results (Youssef et al., 2000). An E2-type mechanism has been proposed that involves adjacent vacant surface sites and the attachment of the alcohol via the hydroxyl group and α-hydrogen atom (Forester et al., 1976).

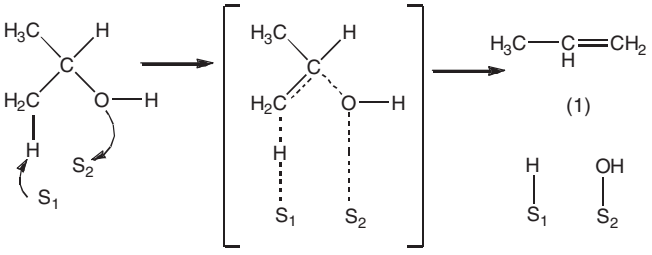

This type of attachment has been reported to involve little strain, even on a plane surface. The adsorbed intermediate species will be located at the site offering an H or OH,

Table 4 Conversion (%) C, $\%S_p$ and $\%S_a$ of selected catalyst as a function of reaction temperature (K). Flow rate 25 cm^3/min.

Catalyst	Reaction temperature											
	533			563			593			623		
	$\%C$	$\%S_p$	$\%S_a$	$\%C$	$\%S_p$	$\%S_a$	$\%C$	$\%S_p$	$\%S_a$	$\%C$	$\%S_p$	$\%S_a$
N4	47	55	45	54	52	48	62	50	50	70	47	53
N8	42	21	79	52	21	78	62	21	79	69	22	78
C4	56	52	48	69	51	49	81	51	49	93	51	49
C8	51	25	75	59	22	78	68	24	76	78	22	78

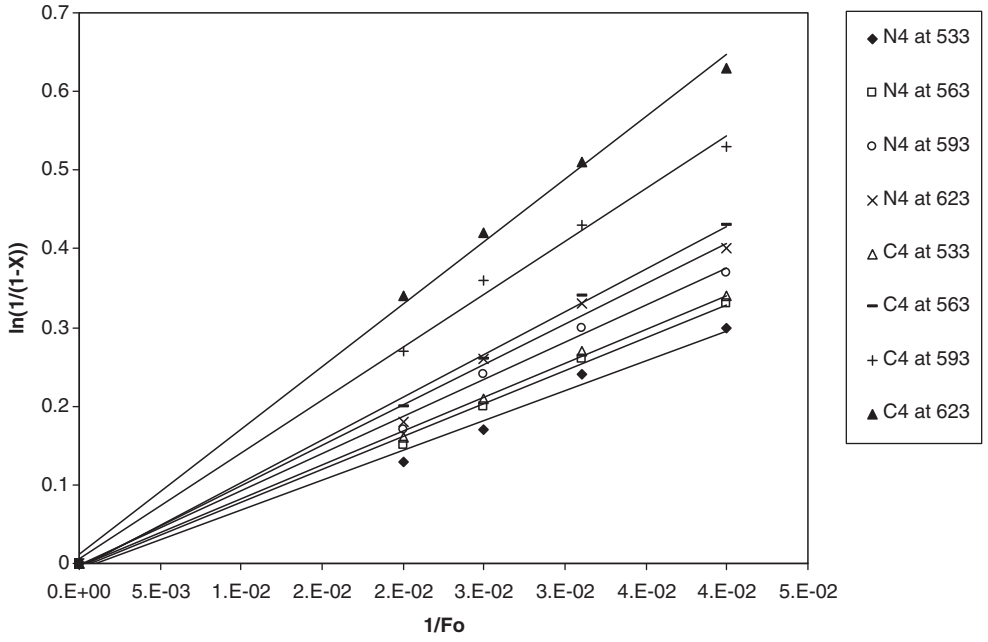

Fig. 5a Application of Bassett–Habgood equation to DHD of isopropanol onto N4 and C4 catalysts at 533–623 K (representative plots).

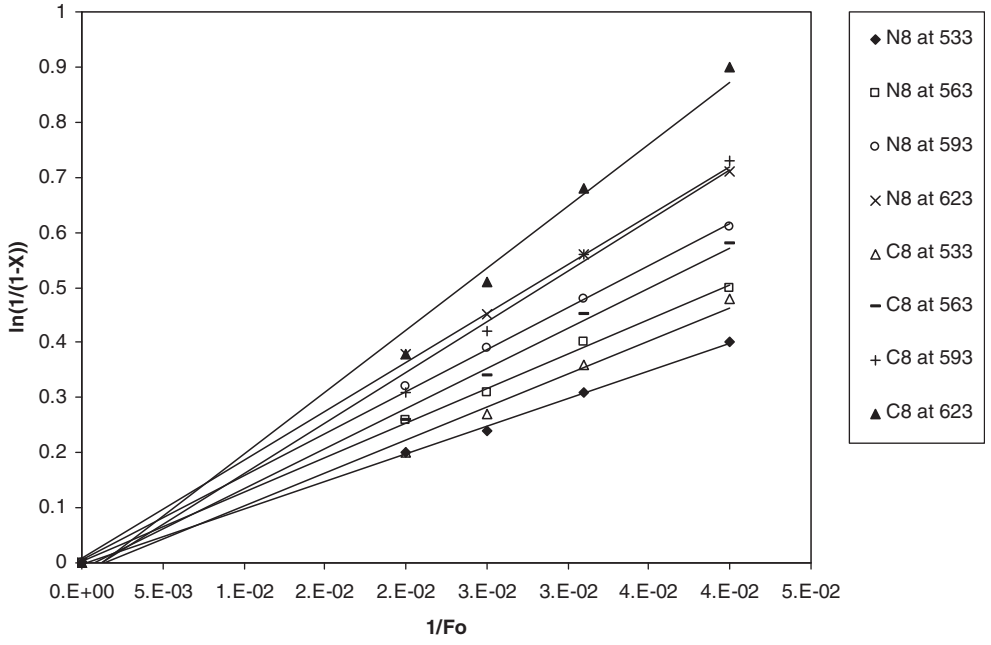

Fig. 5b Application of Bassett–Habgood equation to DHD of isopropanol onto N8 and C8 catalysts at 533–623 K (representative plots).

Table 5 Apparent first order rate constants k_{DHD} and k_{DHG} at 533–623 K for N4, N8, C4 and C8 catalysts.

Catalyst	k_{DHD} (min^{-1})				k_{DHG} (min^{-1})			
	533 K	563 K	593 K	623 K	533 K	563 K	593 K	623 K
N4	7.5	8.3	9.3	10.0	6.0	7.0	9.3	11.5
N8	2.3	3.0	3.5	4.0	10.0	13.0	16.8	19.3
C4	8.5	10.8	13.3	15.8	7.3	10.5	12.8	15.5
C8	3.5	4.0	4.3	4.8	12.0	14.5	18.3	23.5

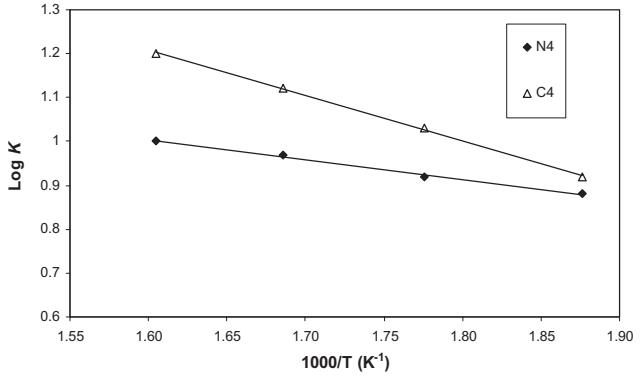

Fig. 6a Representative Arrhenius plots for catalytic DHD of isopropanol.

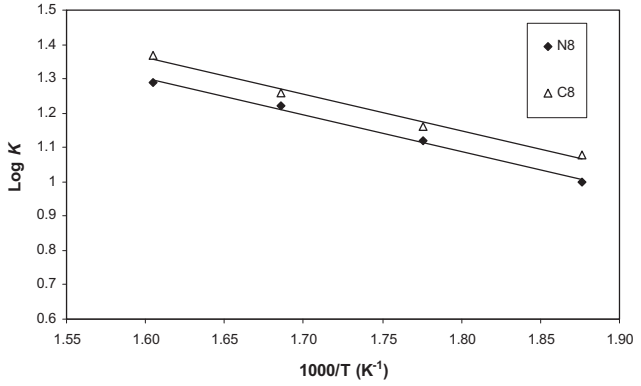

Fig. 6b Representative Arrhenius plots for catalytic DHG of isopropanol.

Table 6 Apparent activation energies (E_a, kJ mol^{-1}) of DHD and DHG of isopropanol over N4, N8, C4 and C8 catalysts.

Catalyst	E_a (kJ mol^{-1}) of DHD	E_a (kJ mol^{-1}) of DHG
N4	11.3	19.8
N8	17.5	20.5
C4	19.1	23.3
C8	15.7	20.5

and consequently it will be primarily involved with the acidic species present on the solid surface (Knozinger, 1985).

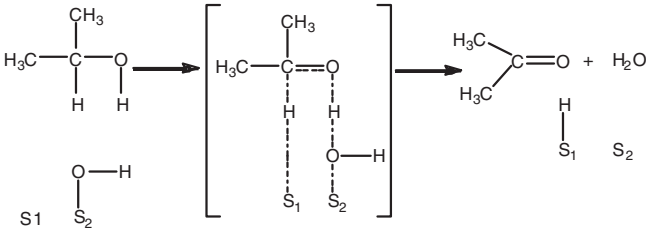

4. Conclusion

The surface properties, catalytic activities, and catalytic selectivities toward isopropanol conversion of NiO/Al_2O_3 and CuO/Al_2O_3 catalysts were investigated.

NiO and CuO were found to exist as highly dispersed phases with crystallite sizes on the nano-scale. Calcination at 823 K did not affect solid–solid interactions to give metal aluminates.

The surface area increased whereas the total pore volume and the mean pore radius increased with the increase of metal loading.

The conversion of isopropanol proceeded via dehydration to propene and dehydrogenation to acetone. Both reactions followed first-order kinetics with the former taking place on surface acid sites and the latter catalyzed by the redox sites.

References

Airaksinen, S.M.K., Krause, A.O.I., Sainio, J., Lahtinen, J., Chao, K.J., Guerreno-Perez, M.T., 2003. Changes of textural and catalytic activity of some transition metal oxides upon loading on alumina. Phys. Chem. Chem. Phys. 5, 4371.

Anderson, I.R., 1957. Structure of Metallic Catalysts. Academic Press, London, UK, p.296.

Ashour, S.S., 2007. Chemisorption and catalytic parameters in relation to the catalytic activity of pure and Na_2O-doped CuO/Al_2O_3 catalysts. Oxford Research Forum J.2 (4), 17–26.

Bassett, D.W., Habgood, H.W., 1960. Gas chromatographic study of catalytic isomerization of cyclopropane. J. Phys. Chem. 64, 769.

Brunauer, S., Emmett, P.H., Teller, E., 1938. Adsorption of gases in multimoleculer layer. J. Am. Chem. Soc. 60, 309.

El-Jamal, M.M., Forissier, M., Auroux, A., 1988. Nature of the B-phase of Bismuth molybdate. J. Chem. Soc. Faraday Trans. 84, 3169.

El-Nabarawy, Th., 1997. Dehydrogenation of cyclohexane in relation to some textural and catalytic properties of Ni/Al_2O_3 and Co/Al_2O_3 catalysts. Adsorp. Sci. Technol. 15 (1), 25.

El-Sharkawy, E.A., El-Hakam, S.E., Samra, S.E., 2000. Effect of thermal treatment on the various properties of iron(111) and aluminium(111) coprecipitated hydroxide systems. Mater. Lett. 42, 333.

Forester, G., Noller, H., Thomke, K., 1976. An E2-type mechanism as applied to the conversion of alcohol over supported transition metal catalysts. J. Catal. 44, 492.

Harlin, M.E., Niemi, V.M., Krause, A.I.O., Weckhuysen, B.M., 2001. Effect of VO_x/Al_2O_3 catalysts in the dehydrogenation of butanes. J. Catal. 203, 67–78.

Knozinger, H., 1985. In: Imelik, B. et al. (Eds.), Catalysis by Acids and Bases. Elsevier, Amsterdam, p. 111.

Leyrer, J., Zaki, M.I., Knozinger, H., 1986. Solid-solid interaction monolayer formation in MoO_3/Al_2O_3 physical mixtures. J. Phys. Chem. 90, 4775.

Lycourghiotis, A., Defosse, C., Delmon, R.M., 1982. Effect of sodium on the cobalt/γ-alumina system. Influence of the preparation conditions and calcination temperature. Less-Common Metals 86, 137.

Mikhail, R.Sh., Youssef, A.M., El-Nabarawy, Th., 1979. Surface properties and catalytic activity of pure alumina and silica-coated alumina. J. Colloid Interface Sci. 70, 467.

Nakamoto, K., 1970. Infrared Spectra of inorganic and Coordination Compounds, second ed. Whiley Interscience, New York.

Sing, K.S.W., 1967. Empirical method for analysis of adsorption isotherms. Chem. Ind. (Lond.) 2, 1520.

Sing, K.S.W., Everett, D.H., Haul, R.A.W., Moscou, L., Pierotti, R.A., Rouguerol, J., Sieminiewska, T., 1985. Reporting physisorption data for gas/solid systems with special reference to the determination of surface area and porosity. Pure Appl. Chem. 57, 559.

Sivaraj, C., Kanatarao, P., 1988. Selective enhancement of surface Cu(+1) species in Cu(11) oxide/zinc oxide/aluminium oxide catalyst. Appl. Catal. 45, 103.

Vishwanthan, V., Rajashekar, M.S., Sreekanth, G., Narayernan, S., 1991. Comparative investigation of hydrogen chemisorption and benzene hydrogenation activity of supported rhodium catalysts. J. Chem. Soc. Faraday Trans. 87 (20), 3449.

Youssef, A.M., Mostafa, M.R., 1988. Isopropanol conversion of chromia–alumina catalysts. Bull. Soc. Chim. Fr. 125, 807.

Youssef, A.M., Ahmed, A.I., Samra, S.E., El-Assey, N.B., El-Sharkawy, E.A., 1998. Textural, structural and catalytic properties of Cr_2O_3/SiO_2 catalysts. Adsorp. Sci. Technol. 16 (3), 175.

Youssef, A.M., Ahmed, A.I., Samra, S.E., El-Assey, N.B., El-Sharkawy, E.A., 2000. Some surface and catalytic properties of V_2O_5–Cr_2O_3/SiO_2, MoO_3–Cr_2O_3/SiO_2 and NiO–Cr_2O_3/SiO_2 ternary solid catalysts. Adsorp. Sci. Technol. 18 (9), 777.

Youssef, N.A., Youssef, A.M., 1991. Catalytic properties of NiO/Al_2O_3 catalysts in relation to their surface characteristics. Bull. Soc. Chim. Fr. 128, 864.